The Astronomical Journal, 165:92 (10pp), 2023 March https://doi.org/10.3847/1538-3881/acb0c7

First Detection of Radio Emission Associated with a Classical Cepheid

L. D. Matthews[1], N. R. Evans[2], and M. P. Rupen[3]
[1] Massachusetts Institute of Technology Haystack Observatory, 99 Millstone Road, Westford, MA 01886, USA; lmatthew@haystack.mit.edu
[2] Center for Astrophysics | Harvard & Smithsonian, 60 Garden Street, Cambridge, MA 02138 USA
[3] National Research Council, 188 Calgary Ave., Penticton, BC, V2A 2T6, Canada
Received 2022 October 14; revised 2023 January 3; accepted 2023 January 4; published 2023 February 9

Abstract

We report the detection of 15 GHz radio continuum emission associated with the classical Cepheid variable star δ Cephei (δ Cep) based on observations with the Karl G. Jansky Very Large Array. Our results constitute the first probable detection of radio continuum emission from a classical Cepheid. We observed the star at pulsation phase $\phi \approx 0.43$ (corresponding to the phase of maximum radius and minimum temperature) during three pulsation cycles in late 2018 and detected statistically significant emission ($>5\sigma$) during one of the three epochs. The observed radio emission appears to be variable at a $\gtrsim$10% level on timescales of days to weeks. We also present an upper limit on the 10 GHz flux density at pulsation phase $\phi = 0.31$ from an observation in 2014. We discuss possible mechanisms that may produce the observed 15 GHz emission, but cannot make a conclusive identification from the present data. The emission does not appear to be consistent with originating from a close-in, late-type dwarf companion, although this scenario cannot yet be strictly excluded. Previous X-ray observations have shown that δ Cep undergoes periodic increases in X-ray flux during pulsation phase $\phi \approx 0.43$. The lack of radio detection in two out of three observing epochs at $\phi \approx 0.43$ suggests that either the radio emission is not linked with a particular pulsation phase, or else that the strength of the generated radio emission in each pulsation cycle is variable.

Unified Astronomy Thesaurus concepts: Cepheid variable stars (218); Stellar mass loss (1613); Radio continuum emission (1340); Stellar atmospheres (1584); Stellar pulsations (1625)

1. Introduction

Classical Cepheid variable stars are yellow supergiants of mass $\sim$4–20 $M_\odot$ whose regular pulsation periods are strongly correlated with their intrinsic luminosities (e.g., Turner 1996). This combination has led to their use as fundamental calibrators of the cosmic distance scale, making these stars of vital importance to extragalactic astronomy and cosmology (Leavitt 1908; Freedman et al. 2001; Di Benedetto 2013, and references therein). They also play a key role in testing stellar evolution models of intermediate-mass stars (e.g., Neilson et al. 2016). However, despite more than a century of study, important gaps remain in our understanding of the physics and evolution of Cepheids.

One of the most confounding puzzles is the decades-old problem known as the "Cepheid mass discrepancy": stellar mass estimates based on theoretical evolutionary models are found to be systematically higher than masses derived observationally from pulsation (via the mass-dependent period–luminosity relation) or from orbital dynamics (e.g., Christy 1968; Pietrzyński et al. 2010). Discrepancies of $\sim$10%–15% have persisted despite continued improvements in models (e.g., Caputo et al. 2005; Keller & Wood 2006; Neilson & Langer 2012). Proposed solutions have included extra mixing, rotation, the need for better radiative opacities, and, perhaps most importantly, mass loss (e.g., Cox 1980; Bono et al. 2006; Neilson et al. 2011, 2012a, 2012b).

If mass loss is occurring during the Cepheid evolutionary phase, this could have important implications for the use of classical Cepheids as distance indicators, since the presence of circumstellar material may add scatter to inferred luminosities in the form of extra extinction in the visible and excess emission at infrared wavelengths (Neilson et al. 2009; Gallenne et al. 2013). Indeed, accounting for these effects may be one of the keys to resolving the discrepancy between the Hubble constant determination from Cepheids compared with that derived from cosmic microwave background measurements (e.g., Riess et al. 2016). Mass loss on the instability strip would also impact other evolutionary aspects of intermediate-mass stars, including whether the star undergoes a blue supergiant phase (e.g., Dohm-Palmer & Skillman 2002; Humphreys 2010; Beasor et al. 2021) and whether the star will end its life as a white dwarf or as a supernova.

Despite the predictions of Cepheid mass loss, the mechanism (s) through which Cepheids may be generating winds and driving significant levels of mass loss (up to $\sim 10^{-6}$ $M_\odot$ yr^{-1}) has remained an unsolved puzzle. Pulsationally driven shocks have been suggested as a candidate (e.g., Willson & Bowen 1986; Neilson & Lester 2008, 2009), but historically there has been little observational evidence linking pulsations with the transport of material to distances well beyond the stellar photosphere where mass loss can occur. However, that has begun to change.

It was recently discovered that the classical Cepheid δ Cephei (δ Cep) exhibits sharp ($\sim\times$4), periodic increases in X-ray emission near pulsation phase $\phi \sim 0.43$ (Engle et al. 2017). This corresponds to the phase just after a radially pulsating Cepheid passes through maximum radius and is near its temperature minimum. The recurrent nature of the X-ray "bursts" at the same phase of δ Cep's pulsation cycle establishes unambiguously that they are pulsationally modulated and not linked to an unseen companion. Evidence of a similar phenomenon has since been seen in the classical Cepheid β Dor (Engle et al. 2017; Evans et al. 2020). The

Table 1
Properties of δ Cephei

α (J2000.0) (1)	δ (J2000.0) (2)	Spec. Type (3)	d (pc) (4)	$\mu_\alpha \cos(\delta)$ (mas yr^{-1}) (5)	μ_δ (mas yr^{-1}) (6)	P (days) (7)	M ($M_\odot$) (8)	$R_\star$ ($R_\odot$) (9)	$T_{\rm eff}$ (K) (10)	$\log\frac{L_\star}{L_\odot}$ (11)
22 29 10.2952 ± 0.0003	+58 24 54.7590 ± 0.0003	F5Iab	255	14.5596 ± 0.1480	3.2375 ± 0.1389	5.366	4.80 ± 0.72	40.0	5960	3.27

Notes. Units of R.A. are hours, minutes and seconds. Units of decl. are degrees, arcminutes and arcseconds. Coordinates and proper motions were adopted from the third Gaia data release (DR3)[a]. Explanation of columns: (1) and (2) R.A. and decl. (J2000.0); coordinates have been referenced to epoch 2018.98 based on the quoted proper-motion values in columns 5 and 6; (3) spectral type; (4) adopted distance in parsecs (Benedict et al. 2007); (5) proper motion in R.A., corrected for the cosine of the decl., in milliarcseconds per year; (6) proper motion in decl. in milliarcseconds per year; (7) pulsation period in days (Fernie et al. 1995)[b]; (8) mass in solar units from Kervella et al. (2019a); (9) mean stellar radius in solar units from Mérand et al. (2015), scaled to our adopted distance; (10) mean effective temperature in kelvin from Fry & Carney (1999); (11) logarithm of stellar luminosity in solar units, derived from $-2.5\log(L_\star/L_\odot) = M_{V,\star} - M_{V,\odot} + \mathrm{BC}$, where the adopted solar absolute V magnitude is $M_{V,\odot} = 4.73$, the stellar absolute V magnitude is taken to be $M_{V,\star} = -4.04 - 2.43(\log P - 1.0)$ (Evans et al. 2013), and the bolometric correction (BC = −0.053) is taken from Flower (1996).

[a] https://gea.esac.esa.int/archive/.

[b] The URL for the database of Fernie et al. (1995) has been updated since the original publication. It is currently available at https://www.astro.utoronto.ca/DDO/research/cepheids/cepheids.html.

origin of the periodic bursts and their implication for δ Cep's atmospheric physics are not presently understood, but the most likely explanation appears to be that the X-ray enhancements originate from either flare-like coronal activity or pulsationally driven shocks (Engle et al. 2017; Moschou et al. 2020). Either phenomenon could play a role in driving Cepheid mass loss.

Centimeter-wavelength radio observations are sensitive to stellar emission from a variety of origins, including free–free emission from ionized winds, chromospheres, and coronae, as well as coronal gyrosynchrotron and gyroresonant emission emission from active regions (e.g., Güdel 2002, and references therein). To gain additional insights into the origin and underlying physics of the δ Cep X-ray bursts and to further explore their possible link with mass loss, we have used the Karl G. Jansky Very Large Array (VLA)[4] to undertake radio-wavelength observations during four observing epochs, three of which were timed to correspond to maximum radius ($\phi \approx 0.43$) during the stellar pulsation cycle. Here we report the successful detection of emission toward the position of δ Cep during one of these latter epochs. We briefly discuss the possible origins of the detected radio emission and its implications for our understanding of the previously discovered X-ray bursts.

2. The Target: δ Cephei

2.1. Basic Properties

δ Cep is the archetype of classical Cepheid variables and is the second closest Cepheid to the Sun (after Polaris). It is a fundamental-mode pulsator with a period of 5.366 days. Some of its additional properties are summarized in Table 1.

δ Cep is believed to be part of a multiple system. HD 213307 (spectral type B7-8 III-IV) is a suspected companion at a projected separation of ∼40″ to the south, and this latter star itself may be a binary with an F0 V companion (Benedict et al. 2002). In addition, Anderson et al. (2015) have reported evidence that δ Cep is a single-lined spectroscopic binary. However, the putative spectroscopic companion has not yet been detected directly. The near-infrared interferometric study of Gallenne et al. (2016) placed constraints on the companion separation and spectral type of $\lesssim$24 mas (<6.1 au) and later than F0 V, respectively. With the availability of Gaia proper-motion data, Kervella et al. (2019a, 2019b) further constrained the nature of the companion, narrowing the spectral type to between K3 V and M0 V. The possible implications of a such a companion for interpreting the radio measurements that we report here are discussed in Section 5.

2.2. Previous Evidence of Ongoing Mass Loss

Several previous studies have provided tantalizing evidence that δ Cep is actively losing mass at a significant rate. Based on infrared imaging observations, Marengo et al. (2010) reported the discovery of an extended nebula and bow-shock-like structure surrounding δ Cep. Bow shocks are generally hallmarks of the interaction between mass-losing stars and the ambient interstellar medium. Therefore, the presence of such a feature is strongly suggestive of a wind and ongoing mass loss. Matthews et al. (2012) subsequently reported the discovery of a nebula of atomic hydrogen (detected through its H I 21 cm line emission) surrounding the stellar position. The H I nebula spans ∼13′ (i.e., a projected size of ∼1 pc), and the combined properties of the nebula and H I line profile are consistent with a wind with a mean outflow velocity of $V_{\rm out} \approx 35$ km s^{-1} and a mass-loss rate between 1.7×10^{-7} and 1.6×10^{-6} $M_\odot$ yr^{-1} after scaling to the distance adopted in the current paper.

Evidence of circumstellar material has also been reported on smaller scales, closer to the photospheric surface of δ Cep. Using near-infrared interferometry, Mérand et al. (2006) found emission extending to 2.4 $R_\star$ that they interpreted as evidence of circumstellar material. Based on optical interferometry, Nardetto et al. (2016) also found excess emission on scales of a few stellar radii, which they suggested may arise from either a circumstellar envelope or nebular material.

3. Observations and Data Reduction

3.1. Pulsation Phase-constrained Observations at 15 GHz

We obtained observations of δ Cep using the VLA during three epochs in late 2018. Each observational epoch corresponded to a separate pulsation cycle and was time constrained to commence within ±15 minutes of the start of pulsation phase $\phi = 0.43$, i.e., just after the passage of the star through

[4] The VLA is a facility of the National Radio Astronomy Observatory (NRAO). The NRAO is a facility of the National Science Foundation operated under cooperative agreement by Associated Universities, Inc.

Table 2
Summary of VLA Observations

Obs. Date (YYYY-MMM-DD) (1)	ν_0 (GHz) (2)	UT Start (hh:mm:ss) (3)	UT Stop (hh:mm:ss) (4)	ϕ (5)	$N_{\rm ant}$ (6)	t (min) (7)	θ_a (arcsec) (8)	θ_b (arcsec) (9)	PA (deg) (10)	$\sigma_{\rm RMS}$ (μJy beam^{-1}) (11)	S_ν (μJy) (12)
2014-Oct-16	10.0	01:12:35	01:46:55	0.31	27	30.3	2.5	1.9	+52	4.3	<12.9
2018-Nov-21	15.0	20:33:19	22:07:58	0.43	26	52.5	2.0	1.5	+85	2.91	<8.7
2018-Nov-27	15.0	05:02:04	06:37:38	0.43	20	56.3	2.2	1.3	−78	2.93	<8.7
2018-Dec-24	15.0	01:18:26	02:49:50	0.43	25	53.8	1.7	1.4	−37	2.76	15.2 ± 2.7
2018-Nov-21/27 combined	15.0	⋯	⋯	0.43	⋯	108.8	2.1	1.4	−84	1.69	<6.1
2018 combined	15.0	⋯	⋯	0.43	⋯	162.6	1.8	1.4	−77	1.69	7.9[a] ± 1.6

Notes. Explanation of columns: (1) observing date; (2) center observing frequency; (3) and (4) UT start and stop times; (5) stellar pulsation phase, computed using the emphemeris from Table 4 of Engle (2014); (6) number of available VLA antennas; (7) total on-source integration time; (8) dirty beam major axis; (9) dirty beam minor axis; (10) dirty beam position angle; (11) rms noise; (12) δ Cep flux density. Data properties are measured from images with $\mathcal{R} = 1$ weighting (see Section 3.1). Source flux densities were derived using Gaussian fits to the images. Quoted upper limits are 3σ.
[a] Value should be regarded as a mean over the duration of the combined data sets.

Table 3
Calibration Sources

Source	α(J2000.0)	δ(J2000.0)	Flux Density (Jy)	ν (GHz)	Date (YYYY-MMM-DD)
3C48[b]	01 37 41.2994	+33 09 35.133	2.6651[a]	10.0	2014-Oct-16
	⋯	⋯	1.7842[a]	15.0	2018-Nov-27
	⋯	⋯	1.7842[a]	15.0	2018-Dec-24
3C286[b]	13 31 08.2880	+30 30 32.959	3.3580[a]	15.0	2018-Nov-21
J2148+6107[c]	21:48:16.0454	+61:07:05.838	0.883 ± 0.002	10.0	2014-Oct-16
J2250+5550[c]	22 50 42.8511	+55 50 14.581	0.321 ± 0.001	15.0	2018-Nov-21
	⋯	⋯	0.260 ± 0.001	15.0	2018-Nov-27
	⋯	⋯	0.258 ± 0.001	15.0	2018-Dec-24

Notes. Units of R.A. are hours, minutes and seconds, and units of decl. are degrees, arcminutes and arcseconds. ν is the frequency at which the flux density in the fourth column was computed.
[a] Flux densities were calculated using the time-dependent coefficients from Perley & Butler (2013). For 3C48, the flux density, S_ν, as a function of frequency was taken to be $\log(S_\nu) = 1.3322 - 0.7688(\log(\nu)) - 0.1952(\log(\nu))^2 + 0.0593(\log(\nu))^3$, where $\nu_{\rm GHz}$ is the frequency expressed in GHz. For 3C286, $\log(S_\nu) = 1.2515 - 0.4605(\log(\nu)) - 0.1715(\log(\nu))^2 + 0.0336(\log(\nu))^3$.
[b] Primary flux calibrator and bandpass calibrator.
[c] Gain calibrator.

maximum radius (see Table 2). The first two observations (on November 21 and 27, respectively) corresponded to contiguous pulsation cycles, while our third observation (on December 24) was separated by a span of five complete pulsation cycles.

Because the nature and origin of any possible radio emission from δ Cep were not known a priori, we chose an observing frequency of 15 GHz (Ku band; $\lambda \approx 2.0$ cm) to provide sensitivity to emission produced by various possible mechanisms, both thermal and nonthermal (see Section 5.2). The Ku band also provides relative ease in calibrating instrumental and atmospheric phase variations.

The 2018 observations were obtained in the VLA C configuration (0.035–3.4 km baselines), providing a sufficiently compact array to minimize the impact of atmospheric fluctuations on gain calibration, but with sufficient spatial resolution to minimize the risk of source confusion. We used the 3-bit correlator mode that allowed three baseband pairs (each with 2048 MHz bandwidth in dual circular polarization), for a total observing bandwidth of ∼6 GHz in dual (right and left) circular polarizations. Each baseband contained 16 subbands, respectively divided into 128 channels of width 1.0 MHz.

During each of the three 2 hr observing sessions, observations of the target star were interleaved with observations of a neighboring point source (J2250+5550) at a projected separation of 3.°9 to provide calibration of the complex gains. The observing sequence involved repeated cycles of ∼80 s on the star and ∼40 s on the calibrator. Additionally, either 3C48 or 3C286 was observed as an absolute flux density calibrator and bandpass calibrator once per session (see Table 3). The data dump time was 2.0 s.

Data processing was performed using the Astronomical Image Processing System (AIPS; Greisen 2003). The archival science data model (ASDM) format files were loaded into AIPS using the BDFIn program from the Obit software package (Cotton 2008). Antenna positions were updated to the best available values. After flagging visibly corrupted data, a requantizer gain correction was applied using the AIPS program TYAPL. Subsequently, a fringe fit was performed using a 1 minute segment of data on the bandpass calibrator (3C48 or 3C286) to correct the instrumental delays. Bandpass calibration was performed in the standard manner, and the absolute flux density scale was calculated by adopting the time-dependent flux density values from Perley & Butler (2013).

Calibration of the frequency-independent portion of the complex gains was performed using a standard approach. First, phase-only corrections were solved for and applied, followed by amplitude and phase corrections. Following some additional flagging of corrupted data, the entire calibration procedure was repeated for each day. Portions of the observing band were

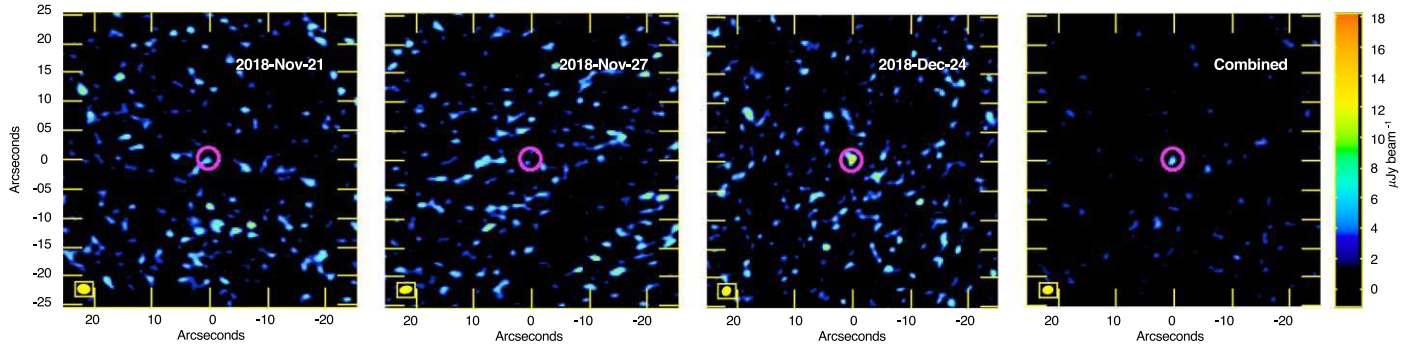

Figure 1. Images of the δ Cep field at 15 GHz obtained with the VLA obtained on three different dates in 2018 (left three images), along with a combined image based on the data from all three epochs (right-hand image). The field of view of each image is 50″. All observations shown were obtained at pulsation phase $\phi \approx 0.43$. The overplotted pink circles are centered on the predicted proper-motion-corrected position of the star and have a diameter of 4″. Statistically significant emission is detected at the stellar position on December 24 (5.5σ) and in the combined image (4.7σ). The synthesized beam is indicated by a yellow ellipse in the lower-left corner of each panel. The image properties are summarized in Table 2.

heavily impacted by radio frequency interference (RFI), leading to overall sensitivity losses of ∼10%. As a final step, the data weights were optimized using the AIPS task REWAY.

As seen in Table 3, the derived flux density of the gain calibrator J2250+5550 is ∼20% higher on 2018 November 21 compared with on 2018 November 27 and December 24. The absolute flux density scale for the November 21 data was set using 3C286, while the latter two days utilized 3C48, which was believed to be undergoing a flare at the time of our observations. It is expected that this flare may contribute uncertainties of up to ∼10% in the Ku band.[5] Part of the discrepancy in the J2250+5550 flux density on different days may also be the result of intrinsic variations in the source itself. We conservatively assume an overall uncertainty of 20% in our absolute flux scale.

Imaging of the fully calibrated data was performed using the AIPS IMAGR task with a Briggs robustness parameter of $\mathcal{R} = 1$ and a cell size of 0.″28. Initially, the data from each day were imaged separately. A combined data set was also created from all three days. The resulting images are shown in Figure 1 and their properties are summarized in Table 2.

3.2. 10 GHz Observation at an Arbitrary Pulsation Phase

In addition to the three epochs of time-constrained observations described above, we analyzed an observation of δ Cep obtained in 2014 under a separate program (14B-196). The 2014 observation was obtained at a slightly lower frequency ($\nu = 10.0$ GHz, X band), also using the C configuration. This observation was executed at an arbitrary pulsation phase ($\phi = 0.31$; see Table 2) and thus does not correspond to the pulsation phase when enhanced X-ray flux has been seen (see Section 1). δ Cep was observed during two scans of ∼17 and ∼13 minutes duration, respectively, interleaved with a series of three observations of the gain calibrator J2148+6107 (see Table 3).

The 2014 measurement used 3-bit sampling in dual circular polarizations. There were two independent baseband pairs, each with a bandwidth of 2 GHz per polarization, for a total bandwidth of 4 GHz. Each baseband was divided into 16 subbands, each with 128 spectral channels. The dump time was 3.0 s.

[5] https://science.nrao.edu/facilities/vla/docs/manuals/oss/performance/fdscale

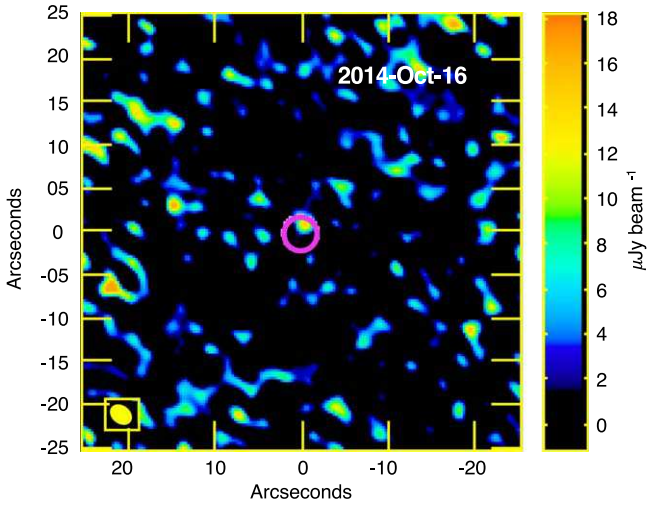

Figure 2. Image of the δ Cep field at 10 GHz obtained with the VLA on 2014 October 16 at pulsation phase $\phi \approx 0.31$. The field of view is 50″. No statistically significant emission was detected from δ Cep during this epoch. The overplotted pink circle has a diameter of 4″ and is centered at the expected position of the star. The brightest positive feature visible within the circle has a significance of $<3\sigma$. The size of the synthesized beam is indicated by a yellow ellipse in the lower-left corner. The image properties are given in Table 2.

Data reduction for the 2014 observations followed the same series of steps as the 2018 observations described in Section 3.1. Like the 2018 data, the 10 GHz observation was significantly impacted by RFI over portions of the observing band, resulting in the need to flag ∼20% of the visibilities.

Imaging of the 2014 data was done in a similar manner to the 2018 data. A cell size of 0.″3 was adopted. The parameters are summarized in Table 2.

4. Results

Figure 2 shows a portion of the 10 GHz image from 2014 October 16, centered on the predicted Gaia proper-motion-corrected source position of the star on this date ($\alpha_{J2000} = 22^h\,29^m\,10.^s290$, $\delta_{J2000} = +58°\,24'\,54.''745$). A circle of diameter 4″ (approximately twice the mean synthesized beam diameter) is overplotted at the source position for reference. No statistically significant emission ($>3\sigma$) is detected at the position of δ Cep. The brightest feature visible within the plotted circle has a significance of $\sim 2.8\sigma$ and, based on a Gaussian fit, it is displaced from the predicted position of the

star by $-1\farcs55 \pm 0\farcs54$ in R.A. and $1\farcs13 \pm 0\farcs34$ in decl. We derive a 3σ upper limit to the δ Cep flux density at 10 GHz of <12.9 μJy (Table 2).

Similarly, during the first two observing epochs of the 2018 observations, no statistically significant emission was detected at or near the expected position of δ Cep (Figure 1). We place 3σ upper limits on the 15 GHz flux density of <8.7 μJy on both days, and based on an image made from the combined November 21 and 27 data we derive a 3σ upper limit of <6.1 μJy (Table 2). However, during the third observing epoch, a point source with a peak flux density of 15.2 ± 2.7 μJy (significance $\sim 5.5\sigma$) is detected at a position consistent with the predicted (proper-motion-corrected) coordinates of δ Cep given in Table 1. Based on a Gaussian fit to the image (using AIPS task JMFIT), the derived position of this feature corresponds to $\alpha_{\rm J2000} = 22^{\rm h}29^{\rm m}10\fs281 \pm 0.011$, $\delta_{\rm J2000} = 58°24'\ 54\farcs965 \pm 0\farcs112$. The position of the source thus agrees with the predicted position of δ Cep in R.A. to within $<1\sigma$ and in decl. to within $<2\sigma$, or approximately 0.1 times the FWHM of the synthesized beam. Assuming that the detected emission arises from δ Cep and not a spatially unresolved companion object (see Section 5.2.6), this represents, to our knowledge, the first reported probable detection of radio continuum emission associated with a classical Cepheid. Dividing the December 24 data into time bins of various durations, we found no evidence for statistically significant variability during the observing window, implying the emission is steady over timescales of a few hours.

Given the rms noise levels in each of our 2018 observations (see Table 2), the source seen in the December 24 data should have been detectable in the other two epochs if its flux density was roughly constant over longer timescales. Assuming a minimum threshold for robust detection of 5σ, we thus infer that the emission detected toward δ Cep must be variable at a level of $\gtrsim$10% on timescales of days or weeks.

As shown in Figure 1 and Table 2, if we average the data from the three observing epochs in 2018, emission is again detected at the expected stellar position. A Gaussian fit yields a source position of $\alpha_{\rm J2000} = 22^{\rm h}29^{\rm m}10\fs299 \pm 0.015$, $\delta_{\rm J2000} = 58°24'\ 54\farcs685 \pm 0\farcs145$, which is consistent with the expected stellar position (Table 1) to within 1σ uncertainties. However, the derived flux density (7.9 ± 1.6 μJy) is smaller than that derived from the December 24 data alone, and the significance of the detection is lower (4.7σ). These results are consistent with no 15 GHz emission being present at the position of δ Cep during the November 21 and November 27 observing epochs at a level of $>3\sigma$ (see above).

Given the small angular size of the synthesized beam in our current observations (see Table 2), the probability of a chance alignment with an extragalactic radio source is expected to be extremely small. For example, at 1.4 GHz, Jackson (2005) estimated the number of extragalactic sources with flux densities $\geqslant 10$ μJy to be 7113 per square degree. Taking the approximation that source counts are roughly similar across centimeter-wavelength bands, this would imply a chance probability of $\sim$0.01% of a random source above that flux threshold appearing within a given synthesized beam for our 15.0 GHz observations. The temporal variability of the source we have detected is also inconsistent with certain classes of extragalactic objects (e.g., normal star-forming galaxies), which tend to be constant in time.

5. Discussion

5.1. Previous Radio Observations of Cepheids

There have been a handful of previous attempts to detect radio continuum emission from classical Cepheid variables (including δ Cep) dating back several decades (Smoliński et al. 1977; Welch & Duric 1988; Drake et al. 1991). One of the original motivations of these studies was the detection of free–free emission from possible ionized outflows from these stars. However, these early efforts were 10–20 times less sensitive than our recent measurements and resulted only in upper limits. Fortunately, the continuum sensitivity of the VLA has since improved by more than an order of magnitude (Perley et al. 2011), enabling far more stringent constraints on emission from stellar sources. Below we discuss several possible scenarios to explain the recently observed 15 GHz radio emission associated with δ Cep.

5.2. Origin of the Observed Radio Emission Toward δ Cephei

5.2.1. Photospheric Emission

Adopting the stellar radius, effective temperature, and distance from Table 1, one can estimate the expected thermal blackbody emission from the stellar photosphere of δ Cep at $\nu = 15$ GHz using the Rayleigh–Jeans approximation: $S_{\rm BB}(15\ {\rm GHz}) = \frac{2\nu^2 k T_{\rm eff}\Omega}{c^2} \approx 1.62$ μJy, where k is the Boltzmann constant, Ω is the solid angle subtended by the star, and c is the speed of light. This is an approximation, since stars are not perfect blackbodies and the exact flux will depend on the radius at which a unity optical depth ($\tau \approx 1$) is reached in the atmosphere for a given wavelength (see, e.g., Drake & Linsky 1986). However, despite these uncertainties, it is clear that photospheric blackbody emission would be well below the detection threshold of our current observations (see Table 2). Furthermore, in contrast with the time-variable nature of the radio source we have detected, photospheric blackbody emission is not expected to vary significantly with time.

Based on the above estimate, we infer that $\lesssim$20% of the radio emission toward δ Cep originates from photospheric blackbody emission from the Cepheid. Since such emission is expected to be optically thick, this also implies that the radio emission that we detected on 2018 December 24 (assuming it originates from δ Cep and not a companion; see Section 5.2.6) arises predominantly from higher regions of the atmosphere.

5.2.2. Free–Free Emission from a Chromosphere/Transition Region

At $\nu = 15$ GHz the emission from the quiet Sun is dominated by optically thick free–free emission from the chromosphere and transition region (e.g., White 2004), whose plasma temperatures lie significantly above those in the photosphere. Previous studies of X-ray emission and optical and ultraviolet emission lines have established that Cepheids too can harbor hot (10^4–10^7 K) plasma indicative of chromosphere-like regions (Kraft 1957; Schmidt & Parsons 1984; Sasselov & Lester 1994a, 1994b; Engle et al. 2014). Chromospheric indicators in Cepheids are generally found to be time variable and pulsation phase dependent, thus pulsationally driven shocks are suspected of being a significant source of heating (e.g., Engle 2014), with possible additional heating from magnetic or acoustic wave dissipation (Sasselov & Lester 1994b).

Adopting the stellar parameters from Table 1 and assuming $r = R_\star$ we estimate a mean, disk-averaged brightness temperature for the 15 GHz emission detected on 2018 December 24 to be ~55,800 K. To put this in context, such a temperature is ~5 times higher than the mean disk-averaged brightness temperature of the quiet Sun at this frequency (Zirin et al. 1991; White 2004). On the other hand, if we assume that the chromosphere of a typical Cepheid extends to several tenths of a stellar radius above the photosphere (Schmidt & Parsons 1984; Hocdé et al. 2020a), the inferred mean brightness temperature would be reduced (e.g., $T_B \approx 25{,}000$ K for a chromospheric radius of $r \sim 1.5\ R_\star$, roughly comparable to the mean values seen in the solar chromosphere during solar maximum; White 2004).

The existence of plasma with temperatures of 25,000–56,000 K associated with δ Cep is consistent with the results of ultraviolet emission-line measurements (Engle 2014). Thus chromospheric free–free emission would appear to be one plausible candidate to explain the observed radio emission from δ Cep. Further, the time-variable nature of Cepheid chromospheres may account for the time-varying nature of radio emission. We note, however, that in this scenario the filling factor (and hence the true brightness temperature) of the radio-emitting plasma is highly uncertain, and that the sources of the radio and ultraviolet emission need not be cospatial (see, e.g., White et al. 1994; Lim et al. 1998). In the chromospheric interpretation the radio emission would be expected to increase in brightness temperature at higher frequencies, hence future quasi-contemporaneous observations in multiple VLA bands could provide further constraints on the viability of this possibility. In principle the spectral index could also be estimated using a single wide observing band. Unfortunately, our present data have an insufficient signal-to-noise ratio to permit a meaningful constraint on the spectral index across the 6 GHz observing passband.

5.2.3. Free–Free Emission from an Ionized Shell

Hocdé et al. (2020b) recently postulated that Cepheids are surrounded by thin shells of ionized gas, with a characteristic thickness of ~15% of the stellar radius and an ionized mass of 10^{-9}–$10^{-7}\ M_\odot$. The authors propose these shells as a means to explain the infrared excesses that have been observed around a number of classical Cepheids, including δ Cep (e.g., Kervella et al. 2006; Mérand et al. 2006; Nardetto et al. 2016). Hocdé et al. (2020b) further speculate that such shells of ionized gas may be linked to the chromospheric activity in Cepheids (see Section 5.2.2), although the temperatures that they propose for the shells based on radiative transfer modeling ($T \sim 3500$–4500 K) are significantly lower than typical chromospheric and transition-region temperatures.

The ionized shells proposed by Hocdé et al. (2020b) are expected to give rise to free–free emission at radio wavelengths. These authors estimate flux densities for five Cepheids discussed in their paper to be in the range 0.01–0.1 μJy at 5 GHz. Although their sample does not include δ Cep, it includes V Centauri (V Cen), a Cepheid with a comparable period ($P = 5.494$ days) but a larger distance ($d = 628.7$ pc). If we take V Cen as a proxy for δ Cep and assume that the radio emission from the shell is optically thick, the expected flux density should scale as $S_\nu \propto d^{-2}\nu^2$. At our observing frequency of 15 GHz, we thus estimate a predicted flux density of ~0.5–5 μJy for δ Cep based on the Hocdé et al. model.[6] These values are ~3–30 times smaller than the emission that we have detected on 2018 December 24. Furthermore, the cool temperatures proposed for the shells in the Hocdé et al. model are inconsistent with the disk-averaged brightness temperature of the observed radio emission if a shell extent of $r \sim 1.15\ R_\star$ is assumed. This model also assumes the shell remains static over time, in contrast with the time-variable emission that we observe. As discussed by Hocdé et al. (2020b), this latter assumption is based on the lack of evidence for time-variability of the infrared excesses around Cepheids.

We conclude that, while in principle the radio emission we observe toward δ Cep may be consistent with a spatially extended ionized shell, limits on the mean electron temperature from the radio emission are inconsistent with the current "cool" ionized shell model proposed by Hocdé et al. (2020b). Part of this discrepancy may result from the fact that the models of Hocdé et al. do not include compression and shocks, which are expected to play a role in heating and ionizing the gas (see also Beĭgman & Stepanov 1981). Inclusion of these effects may also help to reconcile the time-variable nature of the radio emission that we observe with the predictions of the ionized shell model.

5.2.4. Free–Free Emission from a Partially Ionized Wind

As discussed in Section 2.2, previous observations have provided evidence that δ Cep is actively losing mass through a stellar wind. Given the relatively low surface gravity of δ Cep ($\log g = 1.91$ in cgs units, i.e., ~0.30% that of the Sun), its high inferred mass-loss rate (up to $\dot{M} \sim 10^{-6}\ M_\odot\ \mathrm{yr}^{-1}$), the presence of circumstellar H I 21 cm emission, and the rather low outflow velocity estimated for the wind ($V_{\rm out} \approx 35\ \mathrm{km\ s}^{-1}$), Matthews et al. (2012) postulated that δ Cep's wind is likely to be predominantly cool and neutral (see also Glassgold & Huggins 1983; Holzer & MacGregor 1985). Nonetheless, the pulsations suspected of driving Cepheid outflows (e.g., Willson & Bowen 1986) are predicted to generate shocks that may propagate beyond the photosphere and lead to partial (and time-variable) ionization of the wind (Fokin et al. 1996; Marengo et al. 2002; Nardetto et al. 2006; Belova et al. 2014). In this case, free–free emission may be detectable at centimeter wavelengths from the partially ionized wind.

In contrast with the case of a static chromosphere or ionized shell where flux density scales with frequency as $S_\nu \propto \nu^2$ (Sections 5.2.2 and 5.2.3), the frequency dependence of the free–free emission from an ionized, expanding wind is less steep (e.g., $S_\nu \propto \nu^{0.6}$ in the case where the density follows an inverse square law; Wright & Barlow 1975; Panagia & Felli 1975). Using the analytic formulae provided by Drake & Linsky (1986) we can translate our measured 15 GHz flux density into an estimate for the mass-loss rate through an ionized wind. Equation (4) from Drake & Linsky (1986) provides an expression to estimate the effective size of the radio emission based on the observing frequency, measured flux density, and the wind temperature. Assuming a canonical ionized wind temperature of 10^4 K yields a radio size estimate for δ Cep of 3.0 mas, or roughly twice the angular diameter of its photosphere. This in turn would imply an optically thick

[6] Hocdé et al. (2020b) do not quote specific radio flux density estimates for the individual stars in their sample. We therefore base our scaled estimates on their quoted range.

wind, consistent with the expectation for cool-wind giants (Drake & Linsky 1986).

Adopting Drake & Linsky's Equation (2) for the mass-loss rate from an optically thick wind and assuming $V_{\rm out} \approx 35$ km s^{-1} (see above) yields an estimated mass-loss rate for ionized gas of $\dot{M}_{\rm ion}^{\rm thick} \approx 4.8 \times 10^{-10}\,M_{\odot}$ yr^{-1}. This is several orders of magnitude smaller than the mass-loss rate for δ Cep that was estimated previously from H I measurements by Matthews (2012; see Section 2.2). Taking the wind parameters from Matthews et al. (2012) and assuming this wind is the source of the observed radio continuum emission from δ Cep, our current measurements thus imply that the ionization fraction must be rather low and also variable, ranging between ~0.0005 (during times when radio emission is detected) and $\lesssim$0.0003 (when no radio emission is seen).

A lower limit to the expected ionization fraction in the δ Cep wind can be estimated from stellar atmosphere models. For example, from the solar abundance models of Kurucz (1979), the ionization fraction expected in the outer layer of the photosphere for a low-gravity ($\log g = 2.0$) star with $T_{\rm eff} = 6000$ K is ~0.00017, comparable to our radio-derived upper limit. We stress, however, that there is currently considerable uncertainty in the empirically derived mass-loss rate for δ Cep, since it depends on several poorly constrained assumptions (see discussion in Matthews et al. 2012). Based on infrared measurements, Marengo et al. (2010) derived rates one to two orders of magnitude smaller than Matthews et al. (2012), i.e., in the range 7.2×10^{-9}–$2.1 \times 10^{-8}\,M_{\odot}$ yr^{-1}, which would imply a higher fractional ionization.[7] However, these latter mass-loss rate estimates assumed a gas-to-dust ratio of 100 and an outflow speed of 100 km s^{-1}, respectively. As discussed by Matthews et al. (2012), this gas-to-dust ratio may be underestimated by an order of magnitude for the circumstellar environments of supergiants (e.g., Skinner & Whitmore 1988; Mauron & Josselin 2011), while the outflow speeds of supergiant winds are more typically a few tens of kilometers per second well below the stellar escape velocity (see also Holzer & MacGregor 1985; Judge & Stencel 1991). These adaptations would bring the mass-loss estimates of Marengo et al. (2010) and Matthews et al. (2012) in much closer agreement (see Matthews et al. 2012 for discussion). We note also that these mass-loss rate estimates derived from the mass of nebular material assume a constant outflow with time. If the mass loss is instead episodic, this may explain why the current mass-loss rate estimated from the ionized gas appears smaller than expected.

5.2.5. Gyroresonant Emission from Active Regions

Engle et al. (2017) suggested that one possible origin for the period-dependent X-ray bursts observed from δ Cep is the occurrence of magnetic reconnection events tied to spatially compact, heated regions covering a small fraction of the stellar surface. If present, such features may also give rise to gyroresonant emission at radio wavelengths, analogous to the emission seen emanating from solar active regions at frequencies of ~3–15 GHz (e.g., White & Kundu 1996). More specifically, in the nonrelativistic limit, low-order harmonics ($s = 2$–4) of the gyrofrequency $\nu_{\rm B}$ are expected to give rise to gyroresonant radio emission at frequency ν, according to $\nu = s\nu_{\rm B} = 2.8 \times 10^{-3}\ sB$ GHz, where B is the magnetic field strength.

Relatively little is presently known about the magnetic fields of Cepheids. While they do possess outer convective zones, based on their long rotational periods (e.g., ~200 days for δ Cep; De Medeiros et al. 2014) Cepheids have generally not been regarded as candidates for strong magnetic fields or rotationally modulated magnetic activity. However, Barron et al. (2022a, 2022b) recently reported magnetic field detections of several Cepheids based on spectropolarimetric observations, including δ Cep, for which Barron et al. (2022a) measured a disk-averaged longitudinal field strength $\langle B_z \rangle = 0.43 \pm 0.19$ G at pulsation phase $\phi = 0.94$.

What conditions would be necessary to explain the observed radio emission from δ Cep as gyroresonant emission? In the event that active regions are present, then the local magnetic strength within such regions would be expected to be significantly higher than the disk-averaged value. Assuming, for example, emission arising from the third harmonic ($s = 3$), the production of radio emission at $\nu = 15$ GHz would require a local magnetic field strength of ~1800 G, i.e., more than three orders of magnitude higher than the disk-averaged field. The strength of the resulting radio emission would then depend on the covering fraction of active regions. Following O'Gorman et al. (2017; see also Drake et al. 1993; Villadsen et al. 2014) we can estimate the filling factor of such regions, $f_{\rm 15GHz}$, by assuming that the observed 15 GHz brightness temperature, $T_{\rm 15GHz}$, can be expressed as

$$T_{\rm 15GHz} = (1 - f_{\rm 15GHz})\,T_{\rm disk} + f_{\rm 15GHz}\,T_{\rm act}, \quad (1)$$

where $T_{\rm disk}$ is the mean stellar disk brightness temperature and $T_{\rm act}$ is the brightness temperature of a typical active region. We assume that the stellar disk is uniform except at the discrete locations where a coronal active region is present. Taking $T_{\rm 15GHz} = 55{,}800$ K (Section 5.2.2), $T_{\rm disk} = 5690$ K (Table 1), and $T_{\rm act} \approx 2 \times 10^7$ K (based on the X-ray measurements of Engle et al. 2017 during maximum radius) we find $f_{\rm 15GHz} \approx 0.0025$. Assuming instead $T_{\rm act} \approx 10^6$ K (comparable to the brightness temperature of gyroresonant emission above active regions on the Sun; White 2004) yields $f_{\rm 15GHz} \approx 0.05$. The latter is comparable to the coverage factor of 2% estimated by Moschou et al. (2020) as necessary to explain δ Cep's X-ray emission via discrete magnetic reconnection events.

Additional observations and modeling will be needed to establish whether the magnetic properties of δ Cep support this interpretation. Barron et al. (2022a) noted that the magnetic field amplitude and morphology of δ Cep are somewhat peculiar and reminiscent of those of certain Am stars, including Sirius A. However, in the case of Sirius A, the magnetic field does not appear to play a role in generating its observed radio emission. For Sirius A the radio flux between wavelengths of ~0.4–9.0 mm is found to be constant in time and to have a mean, disk-averaged brightness temperature consistently below that of the photosphere (White et al. 2018, 2019). These characteristics are well reproduced by an LTE model of Sirius's photosphere extended to radio wavelengths and are consistent with free–free rather than gyromagnetic emission (White et al. 2018).

[7] Values have been rescaled assuming a distance of 255 pc and a stellar space velocity of 10.3 km s^{-1} (Matthews et al. 2012).

5.2.6. Emission from a Close-in Companion

As discussed in Section 2.1, there is evidence that δ Cep has at least two stellar companions. One of these, HD 213307 (a B7-8 III-IV star with its own possible F0 V companion), lies at a projected separation of $\sim 40''$ and is therefore spatially well resolved from δ Cep in our 2018 VLA observations. No radio statistically significant radio emission was detected at the position of HD 213307 during any of our VLA observing epochs. Using the combined 15 GHz image from our 2018 observations (see Table 3), we place a 3σ upper limit on the quiescent radio emission from HD 213307 to be <5.1 μJy.

The second candidate companion to δ Cep (believed to be a K3 to M0 dwarf; see Section 2.1) lies at a projected angular separation of $\lesssim 24$ mas (Anderson et al. 2015). This is only a small fraction of the synthesized beam in our VLA observations (see Table 3), and thus we cannot spatially resolve δ Cep from this putative companion. Could it be the source of the observed time-varying radio emission?

The coronae of cool, late-type dwarfs frequently give rise to both *quiescent* radio emission and *flares* at centimeter wavelengths (e.g., Güdel 2006). Given the relatively young age of δ Cep ($\sim$80 Myr; Matthews et al. 2012), its close companion would likely be a rapidly rotating, magnetically active star, similar to those found in the Pleiades (Güdel 2002; Engle et al. 2017), making it a plausible radio emitter. However, the characteristics of the observed radio emission do not seem to fit neatly with such an interpretation.

The radio emission detected toward δ Cep on 2018 December 24 does not exhibit any of the typical hallmarks of flaring or bursting emission from a cool dwarf (see, e.g., Bastian et al. 1990; Güdel 2002; Osten & Bastian 2006; Osten & Bastian 2008); for example, we do not see any temporally discrete features (either narrow band or broad band) attributable to bursts or flares visible in the dynamic spectra (see Osten & Bastian 2008; Lynch et al. 2015; Route & Wolszczan 2016), and we find no evidence of temporal modulation of the radio emission over the course of the December 24 observation. The detected emission also does not exhibit any detectable level of circular polarization, as is commonly seen in both flaring and quiescent emission from cool dwarfs at $\nu \lesssim 10$ GHz (e.g., Osten & Bastian 2008; Villadsen & Hallinan 2019), although we note that detectable circular polarization appears to be less common at $\nu \approx 15$ GHz compared with radio frequencies $\lesssim$10 GHz (e.g., White et al. 1994; Osten et al. 2006; Fichtinger et al. 2017).

In contrast to bursts or flares, quiescent emission from cool, low-mass dwarfs is expected to be broad band and vary slowly on timescales or hours or days, consistent with the source that we observe. The typical radio luminosities of such stars are 10^{12}–10^{16} erg s^{-1} Hz^{-1} (Güdel 2006), also consistent with our data: the observed flux density of the source we detect on 2018 December 24 corresponds to a radio luminosity $L_{\rm R} \approx 1.2 \times 10^{15}$ erg s^{-1} Hz^{-1}. However, other properties of the data do not seem to fit this picture.

Assuming that the radio emission from a cool dwarf is optically thick at 15 GHz (e.g., White et al. 1994), the inferred radio brightness temperature, T_B, equals the mean electron temperature (T_e), while in the optically thin case T_B is a lower limit to T_e (e.g., Güdel et al. 1995). Adopting fiducial radii $r \sim 0.8\,R_\odot$ for a K3 V star and $\sim 0.6\,R_\odot$ for an M0 V star, respectively (Lang 1991), the 15.2 μJy flux density we measure at 15 GHz translates to a disk-averaged brightness temperature of $T_B \gtrsim (1.4$–$2.5) \times 10^8$ K—significantly hotter than a typical corona. If instead the emission arises from material extending to $r \sim 2$–3 $R_\star$ with a near-unity filling factor, the temperature estimates ($T_B \sim (2$–$6) \times 10^7$ K) are more in line with typical coronal temperatures of active K and M dwarfs as derived from X-ray observations (White et al. 1994; Giampapa et al. 1996). However, persistent plasma temperatures of $>10^7$ K are inconsistent with X-ray measurements of the δ Cep system.

The X-ray observations presented by Engle et al. (2017) did not have the spatial resolution to separate δ Cep from a source with an angular separation of <24 mas, and therefore these measurements effectively provide an upper limit to the X-ray luminosity and temperature of any such companion. However, the plasma temperatures inferred from the quiescent X-ray emission toward δ Cep by Engle et al. ($T_e \sim 10^6$ K) are more than an order of magnitude smaller than the brightness temperature that we derive from the radio emission under the assumption that it arises from a region with a radius comparable to that of a cool dwarf corona. The only times plasma temperatures are observed to exceed 10^7 K in the environs of δ Cep are during the periodic bursts at pulsation phase $\phi \approx 0.43$. However, Engle et al. (2017) have shown that these temperatures appear to be linked with the atmosphere of δ Cep itself, not a dwarf companion.

The radio/X-ray temperature discrepancy could potentially be reconciled if the X-ray-emitting plasma and the electrons responsible for the radio emission at 15 GHz are not cospatial. However, the dwarf companion to δ Cep would then be atypical of cool dwarfs in exhibiting a disk-averaged brightness temperature at radio wavelengths that is an order of magnitude higher than the plasma temperatures inferred from X-ray measurements. Indeed, for a sample of K and M dwarfs observed at 15 GHz, White et al. (1994) found the stars to be systematically *underluminous* in the radio compared with a model in which the 15 GHz radio emission arises from optically thick gyroresonant emission with a plasma temperature equal to that inferred from X-ray measurements (see also Osten et al. 2006).

Based on these considerations, we conclude that while a cool dwarf companion cannot yet be ruled out as the origin of the radio emission associated with δ Cep, it does not appear to be the most likely candidate. Additional epochs radio observations of the star, both near maximum radius ($\phi \approx 0.43$) and at other (arbitrary) pulsation phases, are needed to obtain additional constraints on this possibility. For example, radio emission that is present only near specific pulsation phases would effectively rule out the companion as the origin.

6. Summary

We have presented multiepoch centimeter-wavelength continuum observations of the classical Cepheid δ Cep obtained with the VLA. The star was undetected in a 10 GHz observation obtained at pulsation phase $\phi = 0.31$ in 2014 October. During late 2018 we obtained additional observations of the star at 15 GHz and a pulsation phase $\phi \approx 0.43$ during three pulsation cycles (two of which were contiguous). The latter phase corresponds to the maximum radius (and minimum temperature) for the star during its 5.366 day pulsation cycle and represents the phase where periodic X-ray bursts have been previously reported. During one of the three epochs (2018 December 24) we detected statistically significant radio emission ($>5\sigma$) consistent with the position of δ Cep. This

represents the first probable detection of radio emission from a Cepheid variable. The nondetection during two other 15 GHz observing epochs implies the emission is variable at a level of $\gtrsim$10% on timescales of days or weeks. This also suggests that the production of radio emission is not tied to a specific pulsation phase, unless the strength of the radio emission produced varies significantly from cycle to cycle. Possible origins for the detected emission include free–free emission from a chromosphere or ionized circumstellar shell, free–free emission from an expanding, partially ionized wind, or gyroresonant emission from localized active regions. The properties of the radio emission do not appear to be consistent with arising from a close-in, late-type (K or M) dwarf companion, although this possibility cannot yet be fully excluded. Follow-up radio monitoring of δ Cep, both during and outside of the phase of maximum radius, will be necessary to further constrain the origin of the radio emission and to determine whether it is correlated with pulsation phase.

We thank the referee for a careful reading of the manuscript. L.D.M. was supported by award AST-2107681 from the National Science Foundation. Support to N.R.E. was provided from the Chandra X-Ray Center NASA contract NAS8-03060. The observations presented here were part of NRAO programs AM1304 (VLA/14B-196) and AM1550 (VLA/18B-005). We thank J. Drake for helpful discussion. This research has made use of the VizieR catalog access tool, CDS, Strasbourg, France (DOI: 10.26093/cds/vizier), the SIMBAD database, operated at CDS, Strasbourg, France, and the data from the European Space Agency (ESA) mission Gaia (https://www.cosmos.esa.int/gaia), processed by the Gaia Data Processing and Analysis Consortium (DPAC; https://www.cosmos.esa.int/web/gaia/dpac/consortium). Funding for the DPAC has been provided by national institutions, in particular the institutions participating in the Gaia Multilateral Agreement.

ORCID iDs

L. D. Matthews https://orcid.org/0000-0002-3728-8082
N. R. Evans https://orcid.org/0000-0002-4374-075X

References

Anderson, R. I., Sahlmann, J., Holl, B., et al. 2015, ApJ, 804, 144
Barron, J. A., Wade, G. A., Evans, N. R., Folsom, C. P., & Neilson, H. R. 2022a, MNRAS, 512, 4021
Barron, J. A., Wade, G. A., Folsom, C. P., & Kochukhov, O. 2022b, arXiv:2207.09255
Bastian, T. S., Bookbinder, J., Dulk, G. A., & Davis, M. 1990, ApJ, 353, 265
Beasor, E. R., Davies, B., & Smith, N. 2021, ApJ, 922, 55
Belova, O. M., Bychkov, K. V., & Rudnitskii, G. M. 2014, ARep, 58, 922
Benedict, G. F., McArthur, B. E., Feast, M. W., et al. 2007, AJ, 133, 1810
Benedict, G. F., McArthur, B. E., Frederick, L. W., et al. 2002, AJ, 124, 1695
Beĭgman, I. L., & Stepanov, A. E. 1981, SvAL, 7, 96
Bono, G., Caputo, F., & Castellani, V. 2006, MmSAI, 77, 207
Caputo, F., Bono, G., Fiorentino, G., Marconi, M., & Musella, I. 2005, ApJ, 629, 1021
Christy, R. F. 1968, QJRAS, 9, 13
Cotton, W. D. 2008, PASP, 120, 439
Cox, A. N. 1980, ARA&A, 18, 15
De Medeiros, J. R., Alves, S., Udry, S., et al. 2014, A&A, 561, 126
Di Benedetto, G. P. 2013, MNRAS, 430, 546
Dohm-Palmer, R. C., & Skillman, E. D. 2002, AJ, 123, 1433
Drake, S. A., & Linsky, J. L. 1986, AJ, 91, 602
Drake, S. A., Linsky, J. L., Judge, P. G., & Elitzur, M. 1991, AJ, 101, 230
Drake, S. A., Simon, T., & Brown, A. 1993, ApJ, 406, 247
Engle, S. G. 2014, PhD thesis, James Cook University
Engle, S. G., Guinan, E. F., Harper, G. M., et al. 2017, ApJ, 838, 67
Engle, S. G., Guinan, E. F., Harper, G. M., Neilson, H. R., & Evans, N. R. 2014, ApJ, 794, 80
Evans, N. R., Bond, H. E., Schaefer, G. H., et al. 2013, AJ, 146, 93
Evans, N. R., Pillitteri, I., Molnar, L., et al. 2020, AJ, 159, 121
Fernie, J. D., Evans, N. R., Beattie, B., & Seager, S. 1995, IBVS, 4148, 1
Fichtinger, B., Güdel, M., Mutel, R. L., et al. 2017, A&A, 599, 127
Flower, P. J. 1996, ApJ, 469, 355
Fokin, A. B., Gillet, D., & Breitfellner, M. G. 1996, A&A, 307, 503
Freedman, W. L., Madore, B. F., Gibson, B. K., et al. 2001, ApJ, 553, 47
Fry, A. N., & Carney, B. W. 1999, AJ, 118, 1806
Gallenne, A., Mérand, A., Kervella, P., et al. 2013, A&A, 558, A140
Gallenne, A., Mérand, A., Kervella, P., et al. 2016, MNRAS, 461, 1451
Giampapa, M. S., Rosner, R., Kashyap, V., et al. 1996, ApJ, 463, 707
Glassgold, A. E., & Huggins, P. J. 1983, MNRAS, 203, 517
Greisen, E. W. 2003, in Information Handling in Astronomy—Historical Vistas, ed. A. Heck (Dordrecht: Kluwer), 109
Güdel, M. 2002, ARA&A, 40, 217
Güdel, M. 2006, arXiv:astro-ph/0609389
Güdel, M., Schmitt, J. H. M. M., & Benz, A. O. 1995, A&A, 302, 775
Hocdé, V., Nardetto, N., Borgniet, S., et al. 2020a, A&A, 641, A74
Hocdé, V., Nardetto, N., Lagadec, E., et al. 2020b, A&A, 633, 47
Holzer, T. E., & MacGregor, K. B. 1985, in Mass Loss from Red Giants, ed. M. Morris & B. Zuckerman (Reidel: Dordrecht), 229
Humphreys, R. M. 2010, in ASP Conf. Ser. 425, Hot and Cool: Bridging Gaps in Massive Star Evolution, ed. C. Leitherer et al. (San Francisco, CA: ASP), 247
Jackson, C. 2005, PASA, 22, 36
Judge, P. G., & Stencel, R. E. 1991, ApJ, 371, 357
Keller, S. C., & Wood, P. R. 2006, ApJ, 642, 834
Kervella, P., Gallenne, A., Evans, N. R., et al. 2019a, A&A, 623, A116
Kervella, P., Gallenne, A., Evans, N. R., et al. 2019b, A&A, 623, A117
Kervella, P., Mérand, A., Perrin, G., & Coudé du Foresto, V. 2006, A&A, 448, 623
Kraft, R. P. 1957, ApJ, 125, 336
Kurucz, R. L. 1979, ApJS, 40, 1
Lang, K. R. 1991, Astrophysical Data: Planets and Stars (New York: Springer-Verlag)
Leavitt, H. S. 1908, AnHar, 60, 87
Lim, J., Carilli, C. L., White, S. M., Beasley, A. J., & Marson, R. G. 1998, Natur, 392, 575
Lynch, C., Mutel, R. L., & Güdel, M. 2015, ApJ, 802, 106
Marengo, M., Evans, N. R., Barmby, P., et al. 2010, ApJ, 725, 2392
Marengo, M., Sasselov, D. D., Karovska, M., Papaliolios, C., & Armstrong, J. T. 2002, ApJ, 567, 1131
Matthews, L. D., Marengo, M., Evans, N. R., & Bono, G. 2012, ApJ, 744, 53
Mauron, N., & Josselin, E. 2011, A&A, 526, 156
Mérand, A., Kervella, P., Breitfelder, J., et al. 2015, A&A, 584, 80
Mérand, A., Kervella, P., Coudé du Foresto, V., et al. 2006, A&A, 453, 155
Moschou, S.-P., Vlahakis, N., Drake, J. J., et al. 2020, ApJ, 900, 157
Nardetto, N., Fokin, A., Mourard, D., & Mathias, P. 2006, A&A, 545, 327
Nardetto, N., Mérard, A., Mourard, D., et al. 2016, A&A, 593, A45
Neilson, H. R., Cantiello, M., & Langer, N. 2011, A&A, 529, L9
Neilson, H. R., Engle, S. G., Guinan, E., et al. 2012a, ApJL, 745, L32
Neilson, H. R., & Langer, N. 2012, A&A, 537, A26
Neilson, H. R., Langer, N., Engle, S. G., et al. 2016, ApJ, 824, 1
Neilson, H. R., Langer, N., Engle, S. G., Guinan, E., & Izzard, R. 2012b, ApJL, 760, L18
Neilson, H. R., & Lester, J. B. 2008, ApJ, 684, 569
Neilson, H. R., & Lester, J. B. 2009, ApJ, 690, 1829
Neilson, H. R., Ngeow, C.-C., Kanbur, S. K., & Lester, J. B. 2009, ApJ, 692, 81
O'Gorman, E., Harper, G. M., & Vlemmings, W. 2017, A&A, 599, A47
Osten, R. A., & Bastian, T. S. 2006, ApJ, 637, 1016
Osten, R. A., & Bastian, T. S. 2008, ApJ, 674, 1078
Osten, R. A., Hawley, S. L., Allred, J., et al. 2006, ApJ, 647, 1349
Panagia, N., & Felli, M. 1975, A&A, 39, 1
Perley, R. A., & Butler, B. J. 2013, ApJS, 204, 19
Perley, R. A., Chandler, C. J., Butler, B. J., & Wrobel, J. M. 2011, ApJ, 739, L1
Pietrzyński, G., Thompson, I. B., Gieren, W., et al. 2010, Natur, 468, 542
Riess, A. G., Macri, L. M., Hoffmann, S. L., et al. 2016, ApJ, 826, 56
Route, M., & Wolszczan, A. 2016, ApJ, 830, 85
Sasselov, D. D., & Lester, J. B. 1994a, ApJ, 423, 777
Sasselov, D. D., & Lester, J. B. 1994b, ApJ, 423, 795
Schmidt, E. G., & Parsons, S. B. 1984, ApJ, 279, 202
Skinner, C. J., & Whitmore, B. 1988, MNRAS, 235, 60

Smoliński, J., Feldman, P. A., & Higgs, L. A. 1977, A&A, 60, 277
Turner, D. G. 1996, JRASC, 90, 82
Villadsen, J., & Hallinan, G. 2019, ApJ, 871, 214
Villadsen, J., Hallinan, G., Bourke, S., Güdel, M., & Rupen, M. 2014, ApJ, 788, 112
Welch, D. L., & Duric, N. 1988, AJ, 95, 1794
White, J. A., Aufdenberg, J., Boley, A. D., et al. 2019, ApJ, 875, 55
White, J. A., Aufdenberg, J., Boley, A. D., et al. 2018, ApJ, 859, 102
White, S. M. 2004, NewAR, 48, 1319
White, S. M., & Kundu, M. R. 1996, SoPh, 174, 31
White, S. M., Lim, J., & Kundu, M. R. 1994, ApJ, 422, 293
Willson, L. A., & Bowen, G. H. 1986, IrAJ, 17, 249
Wright, A. E., & Barlow, M. J. 1975, MNRAS, 170, 41
Zirin, H., Baumert, B. M., & Hurford, G. J. 1991, ApJ, 370, 779